Laboratori Nazionali di Frascati

LNF-67/70

G. Barbiellini, T. Letardi and R. Visentin : ANGULAR DISTRIBUTION OF ELECTRON PAIRS PRODUCED BY POLARIZED PHOTONS AT THE FRASCATI ELECTROSYNCHROTRON.

Estratto da : Nuovo Cimento 51A, 1124 (1967)

C. BARBIELLINI, *et al.*
21 Ottobre 1967
Il Nuovo Cimento
Serie X, Vol. 51 A, pag. 1124-1132

Angular Distribution of Electron Pairs Produced by Polarized Photons at the Frascati Electrosynchrotron.

C. BARBIELLINI, T. LETARDI and R. VISENTIN
Laboratori Nazionali del CNEN - Frascati

F. GRIANTI
Istituto Nazionale di Fisica Nucleare - Sezione di Genova

(ricevuto il 22 Luglio 1967)

Precise measurements of photon polarization in the energy range of 100 to 1000 MeV offer some difficulty because of the lack of a simple physical process to be used as good polarimeter for γ-rays of such an energy. As shown by MAXIMON and OLSEN [1], electron-positron pair production can give information on photon polarization state. The major difficulty, using electron pair production as polarimeter, arises because of the small angular aperture of the pair, at this relatively high energy, as well as the multiple scattering of the produced pair in the converter that averages the natural angular distribution.

In order to acquire detailed knowledge on the possibility of the electron pair production to be used as a proper polarimeter we have done a measurement of 150 MeV photon polarization by measuring the angular distribution of the electron pair by using two wide-gap spark chambers placed beside the Frascati pair spectrometer.

1. – The experimental apparatus.

The polarized γ-ray beam, whose polarization we analise, is the coherent bremsstrahlung beam from the 1 GeV electrons striking a diamond target. This beam is now a facility of the Frascati electronsynchrotron.

The γ-beam is transferred from a synchrotron straight section to the aluminium converter placed within the pair spectrometer as sketched in Fig. 1. The goniometer which holds the diamond target is within the straight section.

As shown in Fig. 1, the beam is collimated twice by the two round collimators C_1 and C_2. C_1 reduces the size of the beam lighting C_2 and decreases the background

(1) L. C. MAXIMON and H. OLSEN: *Phys. Rev.*, **126**, 310 (1962).

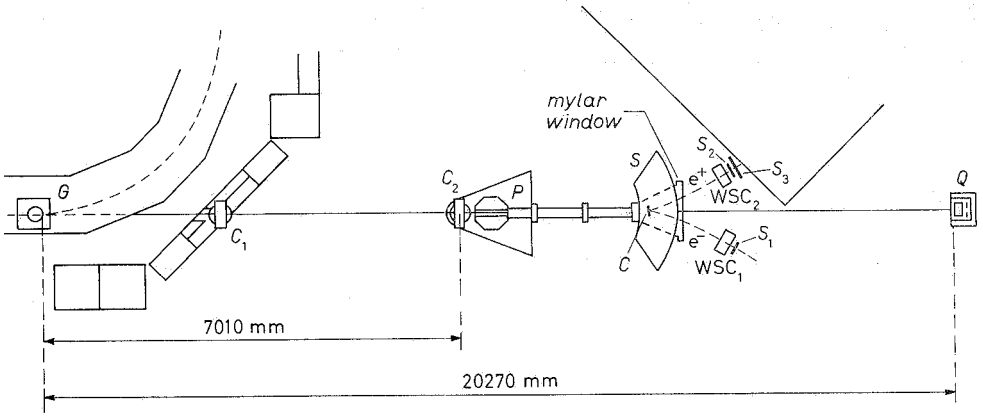

Fig. 1. – Experimental apparatus: G) goniometer; C_1) I collimator, $\varnothing = 5$ mm; C_2) II collimator, $\varnothing = 3$ mm; PS) pair spectrometer; S_1, S_2, S_3) plastic scintillation counters; WSC_1, WSC_2) wide-gap spark chambers; P) clearing field; Q) quantameter.

source. C_2 gives the effective collimation, that is

$$\theta_{\text{coll}} = \frac{1.5 \text{ mm}}{7010 \text{ mm}} \simeq 2.1 \cdot 10^{-4} \text{ rad} ,$$

where θ_{coll} is the collimation half-angle. In the aluminum converter C the γ-beam produces electron-positron pairs. The converter C is only 10 μm thick, in order to reduce the multiple scattering suffered by the produced pairs. The detecting apparatus is also shown in Fig. 1.

The master coincidence between the scintillation counters S_1, S_2, S_3, defining the energy of the symmetric pair (Fig. 2) triggers the Marx generator that applies a

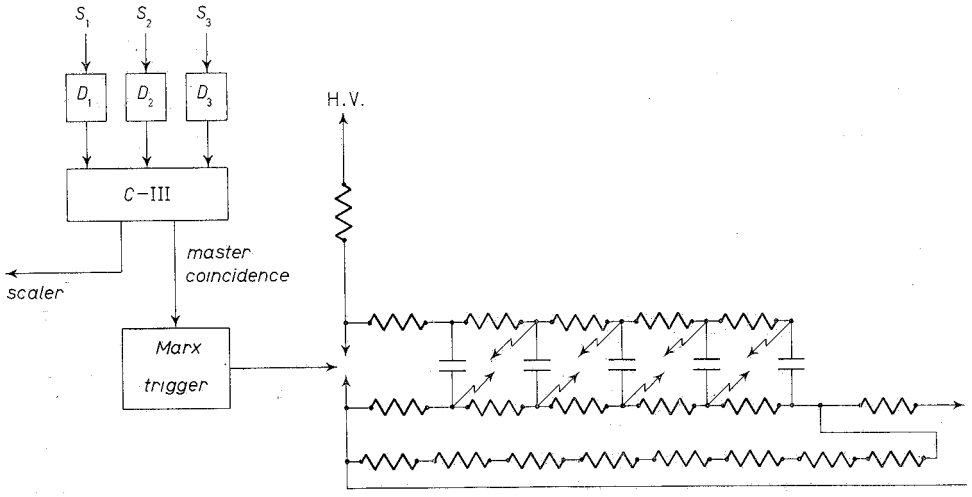

Fig. 2. – Electronic scheme to fire the wide-gap spark chambers: D_1, D_2, D_3) discriminators; C_1 III) threefold coincidence. The Marx generator output goes to the wide-gap spark chamber (WSC).

high-voltage pulse to the wide-gap spark chambers. The two wide-gap spark chambers, used in the delineating mode of operation, detect the track left by the electrons triggering the coincidence.

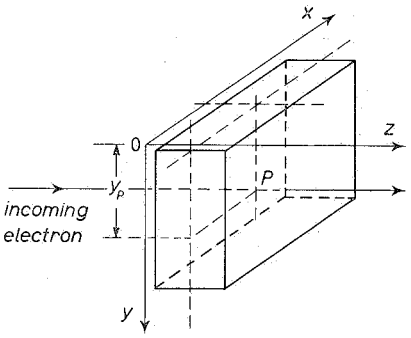

Fig. 3. – Schematic view of the reference frame used to locate the track light by the electron in the WSC.

The wide-gap spark chambers WSC_1, WSC_2 ($(20\times20\times10)$ cm^3) had thin aluminum foils (0.5 mm) as electrodes, and were continuously fluxed with pure He gas, contained in a rectangular mylar box placed between the electrodes.

Linear fiducial marks define a rectangular frame of reference and the position of the track along the y-axis is measured as shown in Fig. 3.

By using mirrors two rectangular views of the chambers were recorded on Ferrania P30 film using a camera with $f/16$ lens opening. The x distribution of electrons was used to check the energy resolution $\Delta E/E$ of the pair spectrometer.

The chambers were pulsed with a 9 kV/cm electric field, applied between the electrodes by a double five-stage Marx generator, with air spark gaps. The total delay between the master coincidence $S_1S_2S_3$ and the H.V. pulse was about 400 ns.

2. – Experimental results.

The γ-beam polarization is defined by the quantity

$$P=\frac{I_\perp-I_\parallel}{I_\perp+I_\parallel},$$

where $I_\perp$ and $I_\parallel$ are the number of photons with electric vector $\boldsymbol{\epsilon}$ perpendicular or normal to the plane $(\boldsymbol{a}_1, \boldsymbol{p}_e)$ respectively, where $\boldsymbol{a}_1$ is the crystal axis (in our case the [110] axis), and $\boldsymbol{p}_e$ is the incoming electron momentum.

At fixed angle θ between $\boldsymbol{a}_1$ and $\boldsymbol{p}_e$, by rotating this plane around $\boldsymbol{p}_e$ it is possible to have any polarization orientation with respect to a fixed reference frame.

We have chosen the angle θ in such a way as to have coherent bremsstrahlung and consequently polarization in the energy region around 150 MeV of the γ-beam energy spectrum.

In order to select the proper photon energy, the symmetric pairs produced by 150 MeV energy photons are magnetically deflected in the pair spectrometer. Due to the magnetic deflection, which

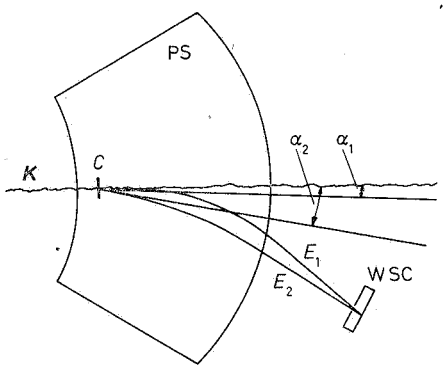

Fig. 4. – Rough sketch to illustrate how two electrons produced at different angles (α_1, α_2), with respect to the photon direction K, and with slightly different energies E_1, E_2 can have the same horizontal co-ordinate at the WSC.

measures the electron pair energy and consequently the photon energy, information on the electron emission angle in the plane normal to the magnetic field $\boldsymbol{B}$ is completely lost. What we measure is thus a projected angular distribution in the plane defined by $\boldsymbol{B}$ and the photon momentum $\boldsymbol{K}$, this plane is coincident with the vertical plane. The same horizontal x co-ordinate at the wide-gap spark chamber can be obtained by electrons of slightly different production angles with respect to the photon direction and simultaneously slightly different energies.

This situation is roughly sketched in Fig. 4. The horizontal co-ordinate is mainly a function of electron energy, and of emission angle too.

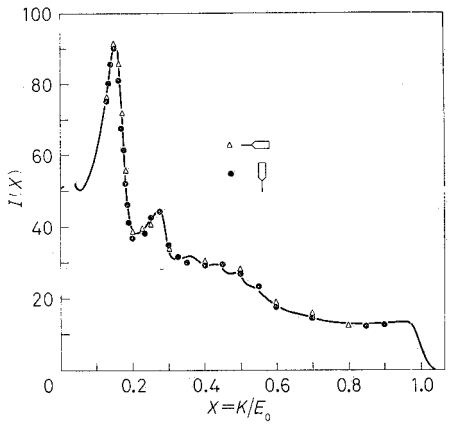

Fig. 5. – Normalized bremsstrahlung intensity of $E_0 = 1$ GeV electrons in the two diamond crystals used alternatively to have vertical and horizontal polarization during the experiment. The two labels refer to each one of the crystals that are rotated around the vertical or the horizontal axis. Solid curve is calculated from ref. (2). X is the fractional energy K/E_0.

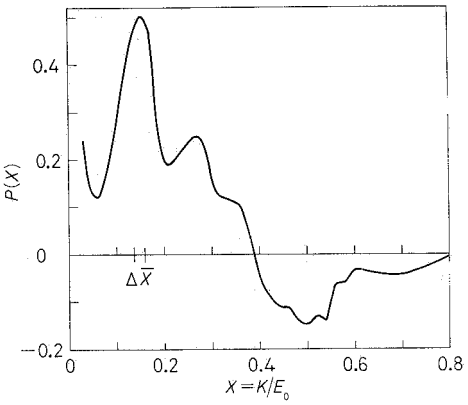

Fig. 6. – Polarization behaviour as a function of the fractional energy X, calculated with diamond in the same situation as for Fig. 5.

We accept small energy average $\Delta E/E$, where E is the electron energy; this is anyway enough to integrate the projected angular distribution in the horizontal plane.

Figure 5 shows the theoretical energy spectrum of the bremsstrahlung intensity (*i.e.* photon energy times number of photons per unit energy interval) from the diamond after the proper orientation has been chosen (2). The experimental intensity values are measured by the pair spectrometer, as in previous experiments (3), while the theoretical spectrum is corrected for the various experimental effects.

The two spectra are obtained from two diamonds used alternatively to change the orientation of the polarization vector $\boldsymbol{\epsilon}$ with respect to the vertical plane. The vertical plane is a priviliged plane because it contains the magnetic field as previously mentioned.

The photon energy resolution $\Delta K/K = \Delta E/E$ (K = photon energy, E = electron energy) of our apparatus is determined by the finite dimensions of the plastic scintillator used to detect the electrons.

---

(2) The best working point of the crystal has been chosen following the prescription of G. Bologna: *Nuovo Cimento*, **40** A, 756 (1967), by taking $\alpha = 13.26°$, $\beta = 0$. Computation of bremsstrahlung spectrum and polarization was performed by the same author.

(3) G. Barbiellini, G. Bologna, G. Diambrini and G. P. Murtas: *Phys. Rev. Lett.*, **8**, 454 (1962); **9**, 46 (E) (1962).

It would be possible to require a better resolution $\Delta K/K$ by reading the horizontal co-ordinate x, which is related to E; however this is not necessary in our case because the polarization value P changes smoothly in the range of the values of K, as defined by the plastic-counter energy resolution ΔK (see Fig. 6).

In Fig. 7 *a*, *b* the distributions of $N_{\parallel}(y)$ and $N_{\perp}(y)$ are plotted.

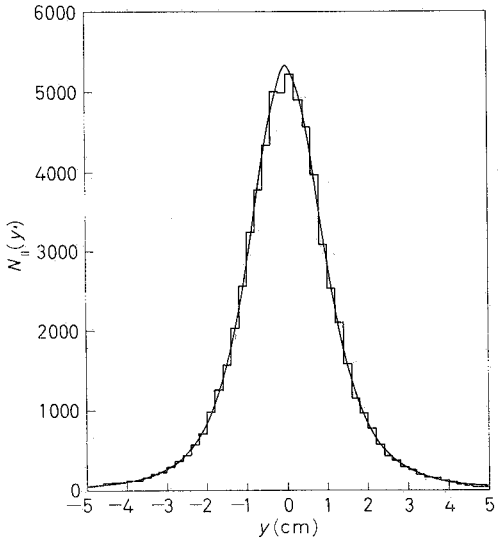

Fig. 7*a*. – Theoretical projected angular distribution $f_{\parallel} = \sigma(1 + P(\sigma_{\parallel} - \sigma_{\perp})/(\sigma_{\parallel} + \sigma_{\perp}))$ at $P = 52\,\%$ after scattering is taken into account and correspondent experimental distribution $N_{\parallel}$. The curve is the theoretical distribution, the histogram is the experimental distribution.

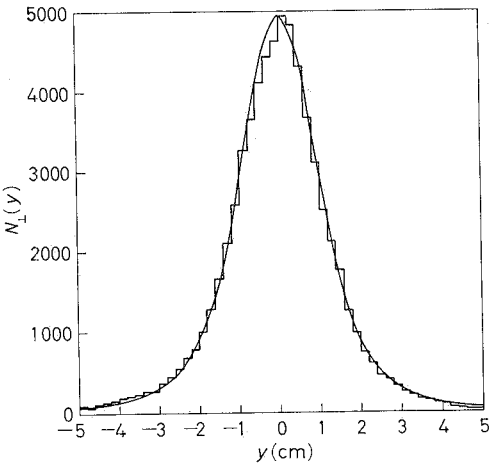

Fig. 7*b*. – Theoretical projected angular distribution $f_{\perp} = \sigma(1 - P(\sigma_{\parallel} - \sigma_{\perp})/(\sigma_{\parallel} + \sigma_{\perp}))$ at $P = 52\,\%$ after scattering is taken into account and correspondent experimental distribution $N_{\perp}$. The curve is the theoretical distribution, the histogram is the experimental distribution.

$N_{\parallel(\perp)}(y)$ are the numbers of events in which one of the electrons of the pair crosses the spark chamber with the co-ordinate between y and $y + \Delta y$, and with the polarization plane coincident with the horizontal (vertical) plane. Due to the small aperture of the pair the vertical y co-ordinate is simply related to the projected angle and to the distance d between the C converter and the scintillation counters ($d \simeq 2$ m). On the other hand, for the same incoming photon flux, we have the following equation:

$$\int_0^\infty N_{\parallel}(y)\,\mathrm{d}y = \int_0^\infty N_{\perp}(y)\,\mathrm{d}y\,,$$

because the total number of events depends only on the total number of incoming photons.

The two distributions $N_{\parallel,\perp}(y)$ are normalized to the same area, *i.e.* to the same number of incoming photons.

The photon polarization is related to $N_{\parallel}(y=0)\Delta y$ and $N_{\perp}(y=0)\Delta y$ through the

equation

$$P = \frac{1}{A}\frac{N_{\parallel} - N_{\perp}}{N_{\parallel} + N_{\perp}} = \frac{1}{A}\frac{R_c - 1}{R_c + 1}, \tag{1}$$

where

$$A = \frac{\sigma_{\parallel} - \sigma_{\perp}}{\sigma_{\parallel} + \sigma_{\perp}} = \frac{R_\sigma - 1}{R_\sigma + 1}, \quad R_\sigma = \frac{\sigma_{\parallel}}{\sigma_{\perp}}, \quad R_c = \frac{N_{\parallel}}{N_{\perp}},$$

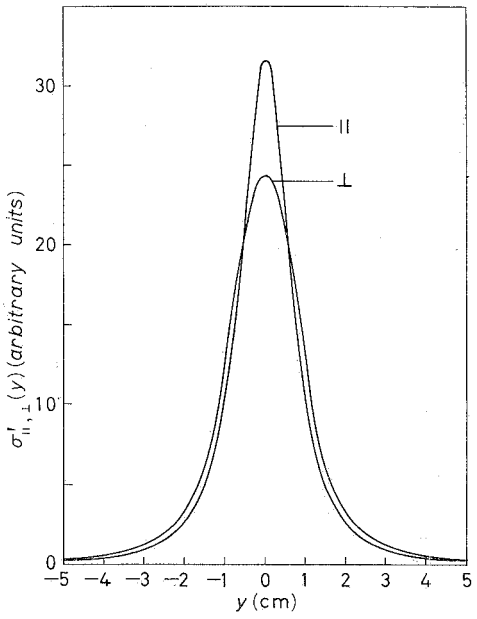

Fig. 8*a*. – $\sigma'_{\parallel,\perp}(y)$ are the theoretical distributions as a function of the vertical co-ordinate y.

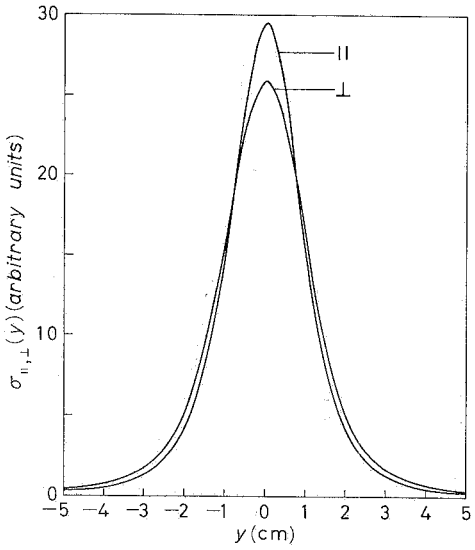

Fig. 8*b*. – $\sigma_{\parallel,\perp}(y)$ are the modification of the distribution shown in Fig. 8*a* after scattering correction is taken into account.

where $\sigma_{\parallel,\perp}$ are the cross-sections for the production of a pair integrated over one of the branches and the production plane of the other branch is parallel or normal to the polarization plane.

The theoretical distribution of the events as function of y and for the two photon polarization states (parallel or normal to the horizontal plane) has been calculated ([4,5]).

Figure 8*a* shows $\sigma'_{\parallel}(y)$, $\sigma'_{\perp}(y)$, the theoretical cross-sections, while Fig. 8*b* shows

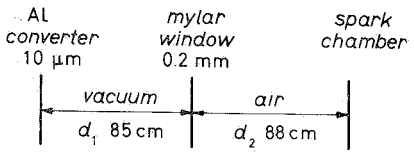

Fig. 9. – Sketch of the scatters met by the electron before detection in the WSC.

([4]) B. ANTONINI: *Thesis* (unpublished).
([5]) M. BARTOLUCCI and F. GRIANTI: Internal Note INFN-66/2 AEB 10 (1(66).

$\sigma_{\parallel}(y)$, $\sigma_{\perp}(y)$ which have been used in eq. (1) and are obtained from $\sigma'_{\parallel,\perp}(y)$ by allowing for multiple scattering in the converter, in the mylar window and in the air gap between mylar window and wide-gap spark chamber.

The smoothing effect of multiple scattering experienced by the electrons in the scatterers placed before the wide-gap spark chamber (see Fig. 9) was evaluated following Molière's theory of multiple scattering by using a simple program for the IBM 7040 computer.

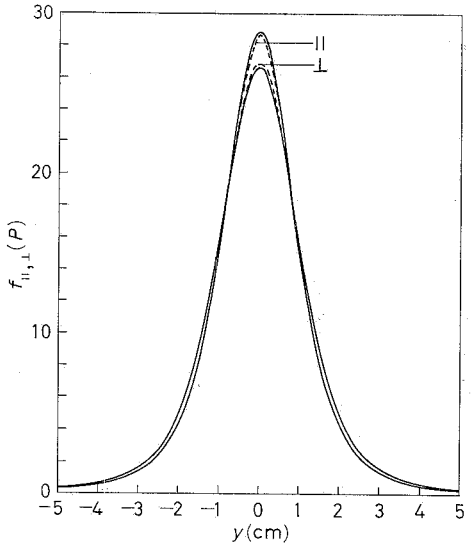

Fig. 10. – Theoretical angular projected distributions $f_{\parallel,\perp}(P, y)$ when scattering is taken into account for the following P values: *a*) continuous line $P = 60\,\%$; *b*) dashed line $P = 40\,\%$. $f_{\parallel,\perp}(P) = \sigma(1 \pm P(\sigma_{\parallel} - \sigma_{\perp})/(\sigma_{\parallel} + \sigma_{\perp}))$.

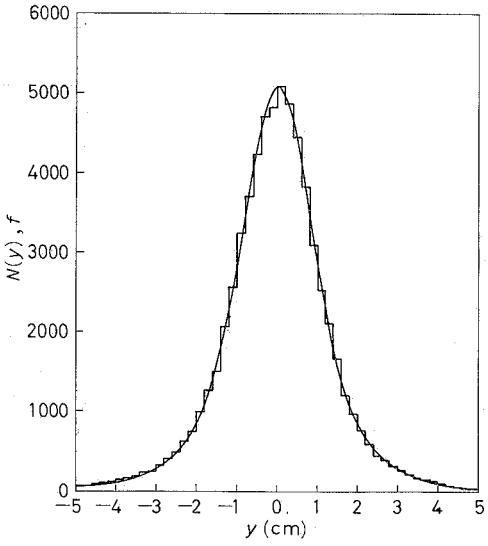

Fig. 11. – Behaviour of the polarization-independent quantities $N(y) = (N_{\parallel} + N_{\perp})/2$ and $f = (f_{\parallel} + f_{\perp})/2$ *vs.* the y co-ordinate. The agreement between the experimental quantity N and the theoretical one f insures that scattering effects are properly evaluated. The curve is the theoretical distribution, the histogram is the experimental distribution.

In Fig. 10 we plot the quantities

$$f_{\parallel,\perp}(P) = \sigma\left(1 \pm \frac{\sigma_{\parallel} - \sigma_{\perp}}{\sigma_{\parallel} + \sigma_{\perp}} P\right).$$

The two sets of curves are referred to $P_1 = 40\%$ (dashed curves) and $P_2 = 60\%$ (continuous curve).

The experimental results $N_{\parallel,\perp}(\Delta y)$, where $N_{\parallel,\perp}$ are previously defined and Δy is the vertical co-ordinate bin ($\Delta y = 2$ mm) are shown in Fig. 7. In the same figure are plotted $f_{\parallel,\perp}(P)$, where $P = 52\%$ is the polarization value which gives the best fit to the experimental points.

Theoretical and experimental values are normalized to the same area. The experimental quantity $N = (N_{\parallel} + N_{\perp})/2$ is also compared to the theoretical quantity $f = (f_{\parallel} + f_{\perp})/2$. Both N and f are polarization-independent. Figure 11 shows the agreement between theoretical prevision and experimental results. This agreement is an internal check that insures that scattering effects are properly taken into account.

The correct scattering evaluation is rather important for polarization measurement because, as shown in Fig. 8*b*, the difference between the $\sigma_{\parallel}$ and $\sigma_{\perp}$ is sensitive to the

TABLE I.

Δy (mm)	R_c	$R_t(P_1)$	$R_t(P_2)$	$R_t(P_3)$
2	1.064 ± 0.016	1.073	1.055	1.083
4	1.062 ± 0.011	1.066	1.050	1.076
6	1.059 ± 0.009	1.057	1.043	1.066

amount of scattering suffered by the electrons.

In the first column of the Table I we give the experimental quantity $R_c(\Delta y) = N_{\parallel}(\Delta y)/N_{\perp}(\Delta y)$ *vs.* different values of Δy; in the second, third, and fourth columns the theoretical ratio $R_t = f_{\parallel}(\Delta y, P)/f_{\perp}(\Delta y, P)$ is represented *vs.* Δy and for the following P values:

$$P_1 = 52\% , \qquad P_2 = 40\% , \qquad P_3 = 60\% .$$

The errors in the values of the first column are only statistical. The values of R_c, $R_t(P_1)$, $R_t(P_2)$, $R_t(P_3)$ *vs.* Δy are shown in Fig. 12.

The beam polarization which we derive from our measurements by using eq. (1) with $\Delta y = 0.4$ cm, is

$$P = (52 \pm 9)\% .$$

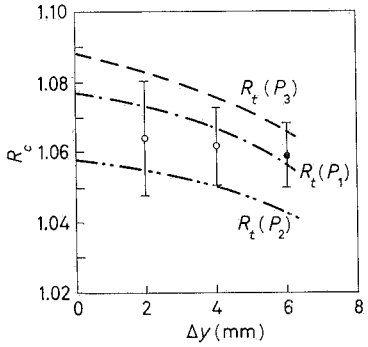

Fig. 12. – Theoretical ratio $R_t(P) = f_{\parallel}/f_{\perp}$ as a function of Δy co-ordinate range around $y = 0$ and for the three values of P corresponding to $P_1 = 52\%$, $P_2 = 40\%$, $P_3 = 60\%$, R_c experimental ratio $N_{\parallel}/N_{\perp}$ *vs.* Δy.

This value is in good agreement with the theoretical value $P = 50\%$ (see Fig. 6).

3. – Conclusions.

A polarization measurement of 150 MeV energy photons using pair production was previously done by counter technique [6].

We believe that the main difference between the two experiments consists in the following:

1) by measuring all the projected angular distributions, with a visualizing technique, we obtain a polarization-independent check, which insures that the scattering effects are properly taken into account (compare the experimental distribution $(N_{\parallel} + N_{\perp})/2$ and the theoretical $(f_{\parallel} + f_{\perp})/2$);

2) the new data are independent from possible electronic inefficiency as the same electronic master is used to detect the events which are polarization-dependent

---

[6] G. BARBIELLINI, G. BOLOGNA, G. DIAMBRINI and G. P. MURTAS: *Phys. Rev. Lett.*, **9**, 519 (C) (1962).

$(N_{\parallel}(y=0),\ N_{\perp}(y=0))$, as well as the normalization factors $\int N_{\parallel}(y)\,\mathrm{d}y$, $\int N_{\perp}(y)\,\mathrm{d}y$, which are polarization-independent.

* * *

The comments, suggestions and assitance of Prof. G. DIAMBRINI, Prof. G. BOLOGNA and Prof. G. P. MURTAS are gratefully acknowledged.

We are grateful also to Ing. F. PANDARESE who helped us in a preliminary automatic scanning of our events.